PCCP

Accepted Manuscript

ROYAL SOCIETY OF CHEMISTRY

www.rsc.org/pccp

Atmospheric chemistry of $(CF_3)_2C=CH_2$: OH radicals, Cl atoms and O_3 rate coefficients, oxidation end-products and IR spectra

Vassileios C. Papadimitriou*[a], Christina S. Spitieri[a], Panos Papagiannakopoulos[a] Mathieu Cazaunau[b], Maria Lendar[b], Véronique Daële[b] and Abdelwahid Mellouki*[b]†

[a]Laboratory of Photochemistry and Kinetics, Department of Chemistry, University of Crete, 71003, Heraklion, Crete, Greece

[b]Institut de Combustion, Aérothermique, Réactivité et Environnement, CNRS/OSUC, Orléans, France

† Electronic supplementary information (ESI) available: ^1H and ^{19}F gas-phase NMR spectra and integrated peaks purity analysis of $(CF_3)_2C=CH_2$; Digitized infrared absorption cross section data for $(CF_3)_2C=CH_2$. See DOI:10.1039/x0xx00000x

Journal: Phys. Chem. Chem. Phys.

*Corresponding authors: Vassileios C. Papadimitriou, e-mail: bpapadim@uoc.gr
Abdelwahid Mellouki, e-mail: mellouki@cnrs-orleans.fr

The rate coefficients for the gas phase reactions of OH radicals, k_1, Cl atoms, k_2, and O_3, k_3, with 3,3,3-Trifluoro-2(trifluoromethyl)-1-propene ($(CF_3)_2C=CH_2$, hexafluoroisobutylene, HFIB) were determined at room temperature and atmospheric pressure employing the relative rate method and using two atmospheric simulation chambers and a static photochemical reactor. OH and Cl rate coefficients obtained by both techniques were indistinguishable, within experimental precision, and the average values were $k_1 = (7.82 \pm 0.55) \times 10^{-13}$ cm^3 molecule^{-1} s^{-1} and $k_2 = (3.45 \pm 0.24) \times 10^{-11}$ cm^3 molecule^{-1} s^{-1}, respectively. The quoted uncertainties are at 95 % level of confidence and include the estimated systematic uncertainties. An upper limit for the O_3 rate coefficient was determined to be $k_3 < 9.0 \times 10^{-22}$ cm^3 molecule^{-1} s^{-1}. In Global Warming Potential (GWP) calculations, radiative efficiency (RE) was determined from the measured IR absorption cross-sections and treating HFIB both as long (LLC) and short (SLC) lived compound, including estimated lifetime dependent factors in the SLC case. HFIB lifetime was estimated from kinetic measurements considering merely the OH reaction, τ_{OH} =14.8 days and including both OH and Cl chemistry, τ_{eff} =10.3 days. Therefore, GWP(HFIB, OH) and GWP(HFIB, eff) were estimated to be 4.1 (LLC) and 0.6 (SLC), as well as 2.8 (LLC) and 0.3 (SLC) for a hundred year time horizon. Moreover, the estimated photochemical ozone creation potential (ε^{POCP}) of HFIB was calculated to be 4.60. Finally, HCHO and $(CF_3)_2C(O)$ were identified as final oxidation products in both OH- and Cl-initiated oxidation, while HC(O)Cl was additionally observed in the Cl-initiated oxidation.

Keywords: OH Kinetics, Cl Kinetics, O_3 Kinetics, Relative Rate Measurements Hydro-Fluorinated Olefins (HFO), IR Absorption Cross Sections, Global Warming Potential (GWP), Estimated Photochemical Ozone Creation Potential (ε^{POCP}), Atmospheric Photochemistry

1. Introduction

The well-established adverse effects of chlorofluorocarbons (CFC) in the stratospheric ozone layer and the climate has led to the search of new, non-ozone depleting substances (non-ODS) as replacements,[1] in accordance to the Montreal Protocol and the subsequent amendments. Several fluorinated compounds have been proposed over the last decade as viable CFC substitutes, such as partially fluorinated alkanes (HFC),[2] ethers (HFE)[3] and alcohols (HFA).[4] However, more recently a new generation of compounds, such as partially fluorinated olefins (HFO), are considered by the industry as sustainable CFC substitutes, since they have suitable physicochemical properties for a wide range of applications (refrigeration, propellants, etc). But prior to use of such fluorinated compounds, it is necessary to assess their environmental impact, and at first to specify the atmospheric fate of these volatile organic compounds upon their release into the troposphere. It is therefore significant to study the gas phase kinetics of these compounds with the primary atmospheric oxidants, i.e., hydroxyl (OH) and nitrate radicals (NO_3), chlorine atoms (Cl), and ozone (O_3), as well as to specify the final oxidation products at tropospheric conditions. Also it should be stressed that the oxidation of fluorinated alkenes is of particular interest for both atmospheric and combustion chemistry.[5] Finally, the ozonolysis of alkenes is known to occur via a complex reaction mechanism that involves the formation of highly reactive Criegee intermediate radicals, and such processes may play a significant role in atmospheric chemistry.[6-8]

Furthermore, the molecular dynamics for the reactions of fluorinated alkenes with OH and NO_3 radicals, Cl atoms and O_3 are of particular importance to the fundamental understanding of such molecular processes. The latter is due to the presence of the olefin double bond and the electronegative nature of F atoms that favor the addition pathways to two sites against the hydrogen abstraction pathways, depending on the temperature and pressure regimes.[9-12] The reaction intermediates and final products of the above reactions may also vary depending on the stereochemistry of the fluorinated alkenes and the temperature and pressures conditions.[13]

The kinetics and mechanism of OH radical reactions with several fluorinated alkenes have been investigated in the past by several experimental studies[14-25] at room temperature and atmospheric pressure, and theoretical studies.[10, 11, 26-28] The reactions of Cl atoms with many fluorinated alkenes have also been examined by several

experimental studies[16, 20, 29] and a few theoretical studies.[10] In addition, the reactivity of NO_3 radicals with several HFOs has also been investigated.[16, 30, 31] On the contrary, the ozonolysis of fluorinated alkenes has not been studied extensively.[25, 32, 33] Several of the above studies have also performed analysis of the final oxidation products.

The present study has measured the rate coefficients for the gas phase reactions of hexafluoroisobutylene ($(CF_3)_2C=CH_2$, HFIB) with OH radicals, Cl atoms and O_3 at room temperature and atmospheric pressure (N_2 or N_2/O_2), employing relative rate methods and using two atmospheric simulation chambers (SC) and the static technique of the thermostated photochemical reactor coupled with an FTIR spectrophotometer (TPCR/FTIR). Furthermore, the final oxidation products of the above reactions were identified at room temperature and 700 (TPCR/FTIR) and 760 (SC) Torr total pressure (N_2/O_2), and the atmospheric degradation mechanism of HFIB was examined. Finally, HFIB radiative efficiency (RE), global warming potential (GWP) and estimated photochemical ozone creation potential (ε^{POCP}) were calculated using the IR absorption cross-sections and OH and Cl rate coefficients measured in the present work, and the atmospheric impact of HFIB is discussed. During the course of the present study, Tovar *et al.*[34] also measured rate coefficients for the reaction of HFIB with Cl and OH at 298 K and 760 Torr , by employing the relative rate method and results are compared and discussed.

2. Experimental

The experimental techniques used, TPCR/FTIR[35] at the University of Crete and two atmospheric simulation chambers[36] at CNRS-Orleans (France), have been presented in detail previously, and only a short description is given herein.

2.1. TPCR/FTIR technique and Relative Rate method

A schematic of the experimental setup is given in Figure 1.

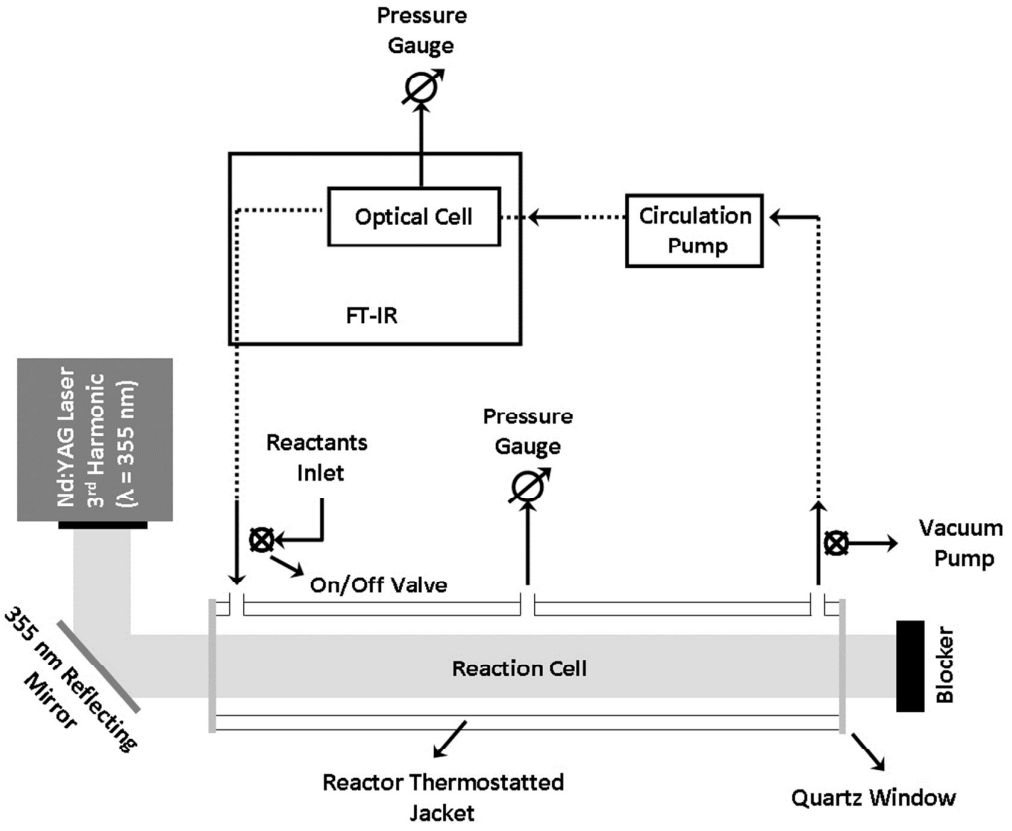

Figure 1. Simplified scheme of the Thermostated Photochemical Reactor apparatus coupled with FTIR Spectroscopy. Dotted lines and arrows show the reaction mixture circulation and homogenization between reaction and optical detection cells. Description of all the components involved is given as inset in the block diagram.

The major components of the TPCR/FTIR apparatus include: a) A 100 cm long jacketed Pyrex reactor of internal diameter, i.d. = 4 cm ($V_{Reactor}$ ~1.2 dm^3), equipped with quartz windows at both ends, so as to be transparent to the UV light and three gas-ports that allow reactants admission, circulation, evacuation and pressure measurement, b) an Nd:YAG laser of which the 3rd harmonic (λ = 355 nm) was used to photolyze the appropriate precursors for producing Cl atoms or OH radicals, c) an FTIR spectrophotometer that hosts the optical cell ($V_{IR\ Cell}$ ~0.1 dm^3) for performing reactants and products analysis and d) a circulation pump that interconnects reactor with optical cell (V_{tubing} ~0.04 dm^3) and ensure the homogeneity of the reaction mixture between the two volumes (20 dm^3 min^{-1} delivery at atmospheric pressure). The experimental room temperature was ~296 ±1 K.

The basic concept in the relative rate method is to monitor the competitive loss of the reactants of interest, i.e., HFIB, and reference compound (ref). The key

condition in relative rate determinations is to ensure that both reactants are solely lost due to their gas phase reaction with OH radicals or Cl atoms and no other sinks or production pathways affect the measured reactants concentrations. The reference reactions for the OH and Cl rate measurements were chosen the well-established reactions of OH with ethylene (CH_2=CH_2), k_4, and Cl + ethylene (CH_2=CH_2), k_5, and Cl + ethane (CH_3CH_3), k_6, respectively. The generic reaction scheme is:

$$\text{X (OH or Cl)} + (CF_3)_2C{=}CH_2 \longrightarrow \text{products}, k \quad (1)$$

$$\text{OH + reference} \longrightarrow \text{products}, k_{ref} \quad (2)$$

and by employing rate laws, it can be proved that the rate coefficients are related via the expression:

$$\ln\left(\frac{[\text{HFIB}]_0}{[\text{HFIB}]_t}\right) = \frac{k}{k_{\text{ref}}}\ln\left(\frac{[\text{ref}]_0}{[\text{ref}]_t}\right) \quad (3)$$

where the indices *0* and *t* refer to the initial and at time *t* concentrations of HFIB and reference compounds, respectively. The reference reaction rate coefficients used were: k_4(296 K, 700 Torr) = 6.97 ×10^{-12} cm^3 $molecule^{-1}$ s^{-1}, k_5(296 K, 700 Torr) = 1.03 ×10^{-10} cm^3 $molecule^{-1}$ s^{-1} and k_6(296 K, 700 Torr) = 5.7 ×10^{-11} cm^3 $molecule^{-1}$ s^{-1}.[37] It is worth to note that that k_4 and k_5 has been determined from the corresponding termolecular expressions at 296 K and 700 Torr.[37] OH radicals were produced inside the TPCR reactor via 355 nm photolysis of CH_3ONO in presence of O_2 and NO, following the reaction scheme:

$$CH_3ONO \xrightarrow{355\,nm} CH_3O + NO \quad (4)$$

$$CH_3O + O_2 \longrightarrow HO_2 + HCHO \quad (5)$$

$$HO_2 + NO \longrightarrow OH + NO_2 \quad (6)$$

CH_3ONO UV cross-section at 355 nm has been determined by Taylor et *al.*[38] to be σ(CH_3ONO, 355 nm) = 2.16 ×10^{-19} cm^2 $molecule^{-1}$ with a dissociation yield of ~0.8. Similarly, Cl atoms were formed via Cl_2 pulsed lased photolysis at 355 nm:

$$Cl_2 \xrightarrow{355\,nm} 2Cl \quad (7)$$

Burkholder et *al.*[39] have measured the UV absorption cross-section of Cl_2 at 355 nm to be σ(Cl_2, 355 nm) = 1.66 ×10^{-19} cm^2 $molecule^{-1}$, with a quantum yield of 2. Note that UV cross-sections and quantum yields are not necessary in measuring the relative rate coefficients, but they are used to estimate the initial concentrations of OH radicals and Cl atoms, given by the expression:

$$[X]_0 = [\text{Precursor}] \times \sigma(\text{Precursor, 355 nm}) \times \Phi_X \times F \quad (8)$$

where [Precursor] represents Cl_2 or CH_3ONO initial concentration, σ(Precursor, 355 nm) is the precursor UV cross-section at 355 nm, Φ_X declares the reactive species production quantum yield and F, the laser fluence in photons cm^{-2}.

In a typical kinetic measurement HFIB, reference compound, Cl_2 or CH_3ONO and synthetic air (80% N_2/O_2) were initially added into the reactor and consequently were mixed for adequate time to ensure homogeneous mixing, both in the reaction and optical cells. The latter was confirmed by monitoring characteristic IR peaks of HFIB during the whole process until less than 1% intensity change to be observed, and mixing time was ~15 minutes. The initial pressure range of reactants was (3.3–28.0) $\times 10^{16}$ molecule cm^{-3} (Cl_2 or CH_3ONO), (2.0 –5.6) $\times 10^{16}$ molecule cm^{-3} (HFIB), (0.6 –8.5) $\times 10^{16}$ molecule cm^{-3} (CH_3CH_3, $CH_3CH_2CH_3$ or CH_2CH_2), and synthetic air (N_2/O_2) was added to reach a total pressure of 700 Torr. Once reaction mixture homogeneity was achieved the infrared absorption spectrum was recorded. Then, the reaction mixture was irradiated to produce Cl atoms or OH radicals and the competitive reactions were initiated. The reaction mixture was initially recycled through the reaction and optical cells during photolysis period, then the circulation was stopped and a second infrared absorption spectrum was recorded, which register the relative losses of HFIB and reference compound. IR spectra were recorded in the range 400 – 4000 cm^{-1} and at 1 cm^{-1} resolution, using 20 co-added scans. Depending on the initial precursor concentration the number of laser photolysis pulses (at 355 nm) was ~1000 – 2000 in order, to yield 5 – 10 % losses for both compounds. Typical laser fluence was 35 mJ $pulse^{-1}$. The photolysis experimental cycle was repeated several times until a ~70 % depletion of both compounds to be reached, where it was possible. Before any kinetic measurement, both reactant and reference compound losses were measured under dark conditions (no laser photolysis) to estimate other probable reactant losses (e. g., wall losses) besides the main reaction. Moreover, the reaction mixtures were also irradiated in the absence of Cl or OH precursors to test any possible photolysis of reactants. In both separate test measurements, no significant fluctuation (<1%) of reactant concentrations was observed. Finally, several experiments were performed using N_2 (no O_2) as bath gas to evaluate the role of O_2. For the OH reactions, the rate coefficients were indistinguishable within experimental precision in the presence or absence of O_2, while for the Cl reactions there was a non-linear behavior. In particular, for O_2 partial pressures lower than 5 Torr, the rate

coefficient plots showed a systematic curvature that was more intense at higher reactants losses. The latter suggests the formation of unstable intermediate adducts, which initiate secondary reactions that lead to additional reactant losses. Therefore, the reported Cl atom rate coefficients correspond to experiments without any such non-linear behavior within experimental precision, by using the appropriate O_2 concentration,

2.2. Atmospheric Simulation Chambers (SC)

Investigations were carried out at 296 ± 2 K and atmospheric pressure in two different collapsible FEP Teflon reaction chambers, with volumes of approximately 7300 and 140 L, respectively. Fans positioned at the lower part of each chamber were ensured the homogeneity. The chambers were surrounded by banks of fluorescent lamps, which provided sources of radiation centered at 254 nm (Philips germicidal lamps TUV, 15W) and 365 nm (Philips, TL 20W/05), respectively. The reaction chambers were approximately half-filled by a diluent gas, typically zero-grade air, via Teflon tubing, using calibrated flow meters. Measured pressures (MKS Baratron capacitance manometers) of the reactants were then expanded into the evacuated vacuum line and isolated in a calibrated mixing bulb, from which they were swept into the reaction chamber by a stream of zero-grade air. HFIB was also introduced via expansion into the chamber from a 0.9 L calibrated reference volume. Concentrated hydrogen peroxide solution was injected directly into the chamber, in the beginning of the experiment, after bubbling N_2 over a 35 % H_2O_2 sample, overnight. Ozone was generated by passing zero-grade air through an ozone generator (Monitor Labs) and was supplied into the reaction chamber. Ozone was detected both via an ozone monitor (HORIBA APOA 370) and FTIR spectroscopy and kinetic results were consistent to each other. Cl_2 was expanded to the 140 L volume chamber from a calibrated volume of 40 L, to an approximate of (5.4 – 6.4) $\times 10^{14}$ molecule cm^{-3}. Reactants were initially introduced into the chamber and then zero-grade air to ca. 760 Torr total pressure was added; the mixture was kept in dark for at least 1 h to allow complete mixing of reactants. A homogeneous reaction mixture was confirmed by consistent, reproducible FTIR or gas chromatographic analysis.

Hydroxyl radicals were generated by the photolysis of hydrogen peroxide:

$$H_2O_2 \xrightarrow{254\ nm} 2\ OH \qquad (9)$$

Molecular chlorine was photolyzed to produce chlorine atoms:

$$Cl_2 \xrightarrow{365\ nm} 2\ Cl \qquad (10)$$

Typical initial mixing ratios for HFIB and references were (3.7 – 4.2) $\times 10^{13}$ (HFIB) and (3.7 – 4.2) $\times 10^{13}$ (C_2H_6) and (2.2 – 3.7) $\times 10^{13}$ (C_3H_8) molecule cm^{-3} in OH measurements and (19.8 – 24.8) $\times 10^{13}$ (HFIB) and (8.7 – 21.1) $\times 10^{13}$ (C_2H_6) molecule cm^{-3} in Cl kinetic measurements, respectively. In ozone rate coefficient determinations, [O_3] was varied between (0.3 – 49.6) $\times 10^{13}$ molecule cm^{-3}, while HFIB was varied between (0.05 – 5.5) $\times 10^{13}$ molecule cm^{-3}. It is worth to note that in the O_3 kinetic measurements, no HFIB reactivity was measured for a single concentration of either compound in excess. Thus only the upper limit for O_3 rate coefficient was determined, by measuring dilution and other possible losses of the reactants inside the chamber. Mixtures of HFIB, reference, and radical precursors were photolyzed until about 50% depletion of the HFIB and/or reference compound were achieved. These conversion levels minimize any complications arising from secondary chemistry and competing reactions of primary photolysis products. The reaction mixtures in Cl rate measurements were analyzed using gas chromatography coupled to a flame ionisation detector (GC-FID, Star 3800 CX, Varian). Sampling volume and dilution were determined to be negligible for Cl kinetic measurements. In OH and O_3 kinetics, reactants and oxidation products are detected in the ppb – ppm range (~10^{12} – 10^{15} molecule cm^{-3}) via a multi-reflection white type mirrors system (143 m path length), which is mounted inside the reactor and interfaced to an FT-IR spectrometer (Nicolet Magna 5700), fitted with mercury cadmium telluride (MCT) detectors. Spectra were recorded over the range 600-4000 cm^{-1} and with a resolution of 1 cm^{-1}. Each resulting spectrum was derived from the co-addition of 130 scans under these conditions. SF_6 was used as a marker in OH and O_3 experiments in order to determine dilution and other possible non-reactive HFIB losses. NOx concentrations were continuously monitored using an online analyzer (HORIBA APNA 360).

2.3 Infrared Absorption Spectra

The infrared absorption spectra of HFIB were determined at 296 ± 1 K over the range 500 to 4000 cm^{-1} using an FTIR spectrometer (JASCO FT/IR-6300). The spectra were measured at 1.0 cm^{-1} resolution, by taking 20 co-added scans in a 16.3 cm long optical

cell, with KBr windows attached at both ends. Absorption cross sections, σ, and integrated bands strengths, *IBS*, were determined using the Beer's law, $A = \sigma \times l \times [HFIB]$, where A represents the absorbance in base *e*, σ, the IR cross-section in cm^2 $molecule^{-1}$, *l*, the optical path length in cm and HFIB concentrations in molecule cm^{-3}. HFIB concentration was determined using absolute pressure measurements and the ideal gas law, while absorbance was varied between 0.05 and 0.7. The HFIB samples were added to the infrared absorption cell from dilute manometrically prepared mixtures in He, with 0.97% and 1.43% mixing ratios varying the total pressure between 10 and 100 Torr. HFIB mixtures were prepared either via turbulent mixing or via freezing HFIB at liquid N_2 temperature and filling round bulb's head space with the required He pressure, in order to minimize systematic errors in mixture preparation method. At least 8 different concentrations were used in the cross section determination for each set of the measurements. HFIB concentrations used were in the range $(0.37–3.05) \times 10^{16}$ molecule cm^{-3}. IR spectra were also recorded at higher resolutions, R =0.5 and 0.25 cm^{-1} with increased co-added scans, to achieve similar sensitivity with the spectra recorded at R =1 cm^{-1}. No significant cross-section dependence on resolution was observed within experimental precision with the exception of the Q-branch peak cross sections, where ca. 5% decrease was measured between the highest and the lowest resolution. IBS values of HFIB were independent of resolution and pressure, therefore may be used to accurately estimate the radiative efficiency.

2.4 Materials

N_2 (UHP, 99.99%) and synthetic air, 80% N_2/O_2, (UHP, 99.99%) were used as supplied. Concentrated H_2O_2 was prepared by bubbling N_2 through a sample that was initially at ~35% mole fraction for a few days. 10 % mixtures of Cl_2 in He were prepared manometrically from pure Cl_2 (Linde, 99.8 %) and He (Linde, 99.996 %).

HFIB (Apollo Scientific, >99.8%), C_2H_6 (Alpha Gaz or Linde, 99.5%), C_2H_4 (Alpha Gaz or Linde, 99.99%), C_3H_8 (Alpha Gaz, 99.8%) and SF_6 (Alpha Gaz, >99.9 %) samples were degassed several times through freeze-pump-thaw cycles at 77 K prior to use. HFIB samples, in particular, were further analyzed using ^1H, ^{13}C and ^{19}F gas phase NMR spectroscopy. Apart from the main HFIB peak, the ^{19}F NMR gas phase spectrum (Figure S1) contained two minor peaks from unknown fluorinated impurities, in the chemical shift range characteristic of $–CF_3$ groups. Assuming the

impurities contain one $-CF_3$ group per molecule, HFIB is calculated to be 98.8% pure, while for two $-CF_3$ group per molecule, HFIB is 99.4% pure. Integration of the ^1H NMR gas phase spectrum showed HFIB to be approx. 98.8% pure (Table S1). Typical gas phase NMR spectra are presented in supporting information (Figure S1). For kinetic measurements, the sample was directly introduced into the reactor from the container since fluorinated impurities at this levels are not expected to have any effect (see error analysis section). The pressure inside the reactor and the optical cell was measured with calibrated differential pressure sensor diaphragms.

3 Results

This section includes the kinetic results for the gas phase reactions of OH radicals, Cl atoms and O_3 with HFIB at 296 K and 700–760 Torr, using both experimental techniques. Moreover, IR cross-sections of HFIB and the end-products analysis for the OH- and Cl-initiated oxidation are presented.

3.1 OH Kinetics

The results and conditions of the relative OH rate coefficient measurements are summarized in Table 1. The rate coefficients represent the average values obtained by both experimental techniques. The quoted uncertainties also include the extremes of the estimated uncertainties for the reference reactions. The precision of rate coefficient measurements was high, and the agreement between both experimental techniques was excellent, validating the reproducibility of our measurements.

Table1. Relative rate ratios and rate coefficients and conditions for the gas phase reaction of OH radicals with $(CF_3)_2C=CH_2$.

Pressure[a] (Torr)	$[(CF_3)_2C=CH_2]$[b]	$[CH_3ONO]$[b,c]	$[CH_2=CH_2]$[b]	r:(k_1/k_{Ref}) $\pm2\sigma$[d]	$k_1\pm2\sigma$[d] (10^{-11} cm^3 molecule^{-1} s^{-1})
Reference Reaction: $OH+CH_2=CH_2$,[37] $k_{CH2=CH2}(296K)=6.97\times10^{-12}$ cm^3 molecule^{-1} s^{-1} (TPCR/FTIR)					
700	18.2	230	10.8	0.11±0.01	7.70±0.30
700	20.1	280	10.8	0.12±0.01	8.07±0.40
700	40.2	268	7.3	0.11±0.01	7.99±0.30
k_1(296 K, 700 Torr)= (7.92 ±0.20) $\times10^{-13}$ cm^3 molecule^{-1} s^{-1}					
Reference Reaction: $OH+CH_3CH_2CH_3$,[37] $k_{CH3CH2CH3}(296K)=1.10\times10^{-12}$ cm^3 molecule^{-1} s^{-1} (SC)					
760	0.33	-	0.32	0.71±0.01	7.54±0.11

760	0.37	-	0.53	0.73±0.01	7.77±0.12
k_1(296 K, 760 Torr)= (7.66 ±0.23) ×10^{-13} cm^3 $molecule^{-1}$ s^{-1}					
Reference Reaction: $OH+CH_3CH_3$,[37] k_{CH3CH3}(296K)=2.50×10^{-13} cm^3 $molecule^{-1}$ s^{-1} (SC)					
760	0.33	-	0.14	3.18±0.06	7.96±0.15
760	0.34	-	0.36	3.16±0.07	7.90±0.16
760	0.34	-	0.37	3.08±0.05	7.71±0.12
k_1(296 K, 760 Torr)= (7.86 ±0.25) ×10^{-13} cm^3 $molecule^{-1}$ s^{-1}					

[a] All experiments performed with synthetic air (80% N_2, 20% O_2) as a bath gas
[b] CH_3ONO, $(CF_3)_2C=CH_2$ and $CH_2=CH_2$ concentrations referred in 10^{15} molecule cm^{-3}.
[c] Dashes in CH_3ONO concentrations column denote that H_2O_2 has been used as OH precursor, which was directly inserted into the chamber via a bubbler.
[d] The quoted uncertainties are at 95% level of confidence and refer only to the precision of the least-square fit of ln ($[(CF_3)_2C=CH_2]_0/[(CF_3)_2C=CH_2]_t$) versus ln ($[CH_2=CH_2]_0/[CH_2=CH_2]_t$)

The plots of expression 3 for OH reactions with HFIB and three reference compounds at T = 296 K and P = 700 Torr (TPCR/FTIR) and 760 Torr (SC) are presented in figure 2. These plots also compare the experimental results obtained by both experimental techniques. Three different reference reactions were used to minimize possible systematic uncertainties stemming from the reference reactions. All reference reactions have been well studied in the past and have rate coefficients comparable to the title reaction, and k/k_{ref} was varied ~30 times (0.10 – 3.2). The latter demonstrates the high sensitivity of our method, because even for the highest and lowest k_{ref} values the derived k/k_{ref} values were identical and very precise. In Figure 2, all three references provide reproducible results and are well represented by straight lines with negligible (almost zero) intercepts, in consistence with expression 3. Rate coefficients were obtained by forcing the fits to pass through zero, in accordance with expression 3 and since the intercepts were negligible and within our experimental precision. The obtained k/k_{ref} values were in agreement within ~3 % for all three reference reactions (see Table 1). For each reference reaction several independent measurements were carried out to evaluate the precision of our measurements. Both precision and reproducibility were high. It is worth to note, that no pressure dependence was observed between 700 and 760 Torr, within measurements precision, indicating that the reaction, in that pressure regime, is approaching the high pressure limit. Therefore, even though the independent rate coefficients determined in the two different facilities were measured at different pressures (700 and 760 Torr), this difference has a non-measurable, if any, effect in reaction kinetics in that regime; thus, an average value at

P =1 atm is quoted in this work, without any pressure correction to be included, since it would probably increase the uncertainties of the quoted rate coefficient values. The average value of all three independent measurements resulted in a rate coefficient k_1(296 K, 1 atm) = (7.82 ± 0.30) ×10^{-13} cm^3 $molecule^{-1}$ s^{-1}. The quoted uncertainties are the 2σ precision of the fits and encompass the uncertainties extremes of each measurement.

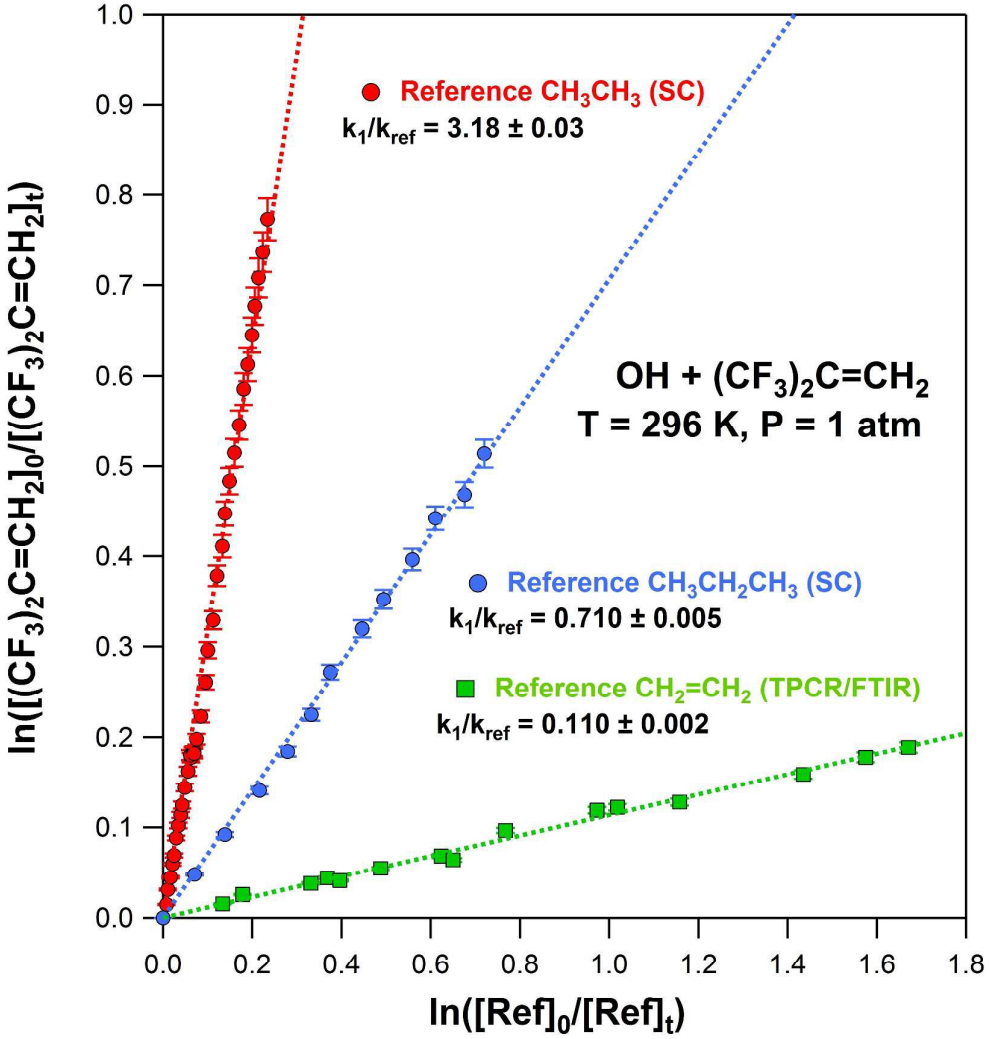

Figure 2. Relative rate data obtained at room temperature, 296 K, and 700 (TPCR/FTIR) and 760 (SC) Torr for the reaction of OH with $(CF_3)_2C=CH_2$ using CH_3CH_3 and $CH_3CH_2CH_3$ and $CH_2=CH_2$ as reference compounds. Synthetic air was used in all measurements. Symbols are explained as insets and dotted lines are linear least-squares fits of the data to equation VII and the average rate coefficient that they yield is k_1(296 K, 1 atm) = (7.82 ±0.30) ×10^{-13} cm^3 $molecule^{-1}$ s^{-1}. Note that reaction system is approaching the high pressure limit at that regime and no substantial differences are expected between 700 and 760 Torr for the rate coefficient (see also

text). The quoted uncertainty is at 95 % level of confidence and encompasses the error limits of the three independent measurements. The error bars represent an upper limit for the precision of the measurements.

3.2 Cl Kinetics

The summary of the experimental conditions and results for the gas phase reactions of Cl atoms with HFIB are presented in table 2. Experiments were carried out using N_2 as bath gas and with O_2 pressures varied between 0 – 140 Torr. At O_2 pressures less than 5 Torr, the kinetic measurements' plots exhibited a curvature indicating that the excited Cl-adduct formed is less stable than the corresponding OH-adduct.[16] Therefore, all Cl kinetic measurements were performed with sufficient amounts of O_2 to inhibit secondary chemistry.

Table 2. Relative rate ratios and rate coefficients and conditions for the gas phase reaction of Cl atoms with $(CF_3)_2C=CH_2$.

Pressure[a] (Torr of O_2)	**$[Cl_2]$[b]**	**$[(CF_3)_2C=CH_2]$[b]**	**[Reference][b]**	**$r_0:(k_2/k_{Ref})$ $\pm 2\sigma$[c]**	**$k_2 \pm 2\sigma$[c] (10^{-11} cm^3 molecule^{-1} s^{-1})**
Reference Reaction: $Cl+CH_3CH_3$,[37] $k_{CH3CH3}(296K)=5.70\times10^{-11}$ cm^3 molecule^{-1} s^{-1} (TPCR/FTIR)					
700	87.5	42.1	71.3	0.60±0.01	3.40±0.03
700	90.7	45.8	84.1	0.61±0.01	3.50±0.03
700 (20)	32.4	39.9	55.0	0.61±0.01	3.46±0.04
700 (5)	127	41.9	73.6	0.60±0.01	3.43±0.04
				k_2(296K, 700Torr)=(3.45±0.08) × 10^{-11} cm^3 molecule^{-1} s^{-1}	
Reference Reaction: $Cl+CH_2=CH2$,[37] $k_{CH2CH2}(296K)=1.03\times10^{-10}$ cm^3 molecule^{-1} s^{-1} (SC)					
700	217	31.9	10.6	0.33±0.01	3.44±0.13
700	156	58.7	8.3	0.33±0.01	3.37±0.04
				k_2(296K, 700Torr)=(3.40±0.17) × 10^{-11} cm^3 molecule^{-1} s^{-1}	
Reference Reaction: $Cl+CH_3CH_3$,[37] $k_{CH3CH3}(296K)=5.70\times10^{-11}$ cm^3 molecule^{-1} s^{-1} (SC)					
760	0.33	0.21	0.09	0.64±0.01	3.66±0.06
760	0.27	0.22	0.14	0.60±0.01	3.42±0.05
760	0.27	0.48	0.21	0.60±0.01	3.45±0.06
				k_2(296K, 760Torr)=(3.51±0.21) × 10^{-11} cm^3 molecule^{-1} s^{-1}	

[a] All experiments performed with synthetic air (80% N_2, 20% O_2) as a bath gas unless otherwise noted

[b] Cl_2, $(CF_3)_2C=CH_2$ and Reference concentrations referred in 10^{15} molecule cm^{-3}

[c] The quoted uncertainties are at 95% level of confidence and refer only to the precision of the least-square fit of ln $([(CF_3)_2C=CH_2]_0/[(CF_3)_2C=CH_2]_t)$ versus ln $([Ref]_0/[Ref]_t)$

Figure 3 shows the plots of expression 3 for Cl atom reactions with HFIB and two reference compounds at T = 296 K and P = 700 and 760 Torr, taken by both experimental techniques. Solid square symbols represent data taken using the

TPCR/FTIR technique, and solid circles data taken using the atmospheric simulation chambers (SC).

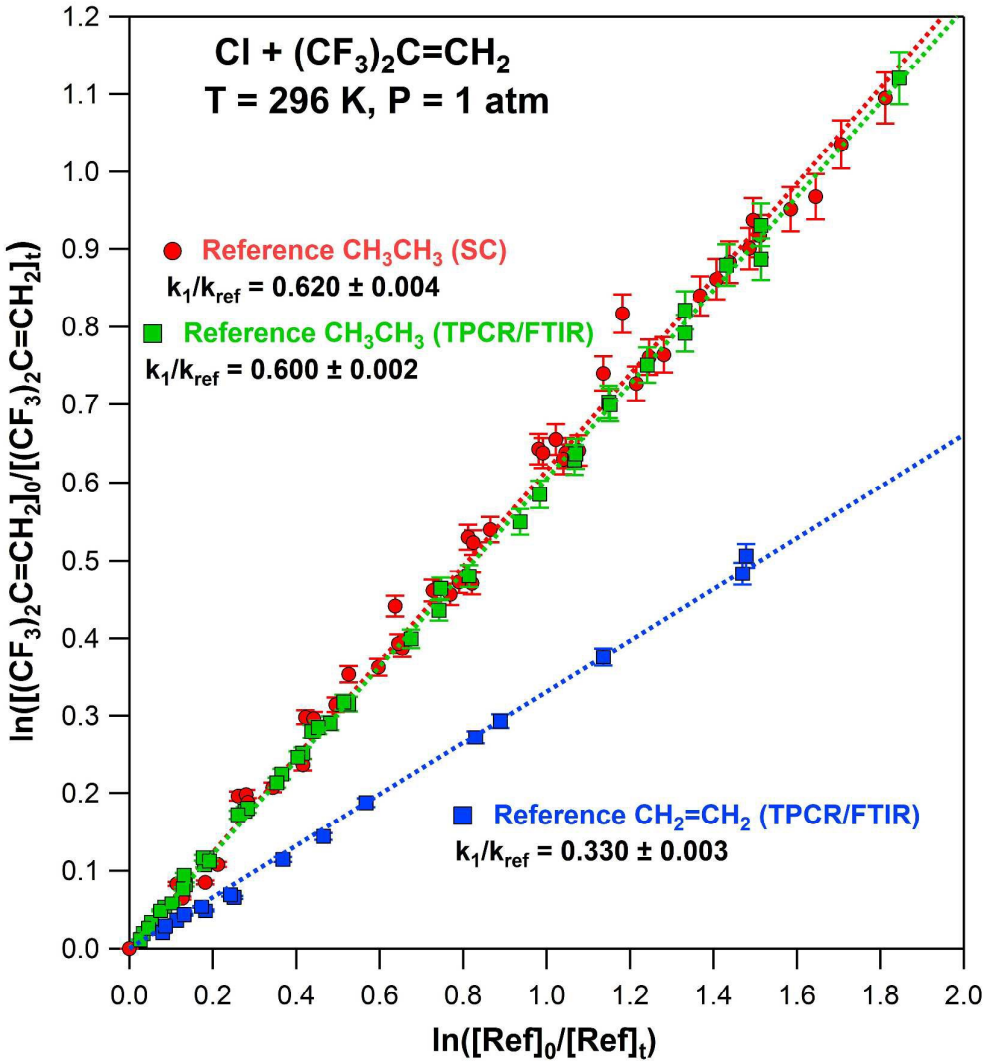

Figure 3. Relative rate data obtained at room temperature, 296 K, and 700 (TPCR/FTIR) and 760 (SC) Torr for the reaction of Cl atoms with $(CF_3)_2C=CH_2$ using CH_3CH_3 and $CH_2=CH_2$ as reference compounds. Synthetic air was used in all measurements. Symbols are explained as insets and dotted lines are linear least-squares fits of the data to equation VII and the average rate coefficient that they yield is k_2(296 K, 1 atm) = (3.45 ±0.10) $\times 10^{-11}$ cm^3 molecule^{-1} s^{-1}. The quoted uncertainty is at 95 % level of confidence and encompasses the error limits of the three independent measurements. The error bars represent an upper limit for the precision of the measurements. Note that reaction system is approaching the high pressure limit at that regime and no substantial differences are expected between 700 and 760 Torr for Cl the rate coefficient (see also text).

Reference reactions were selected such as the k/k_{ref} ratios, for the two different reference compounds to be relatively close to unity and to differ by a factor of ~2,

($k_{CH3CH3}/k_{CH2=CH2}$) in order to evaluate the sensitivity of our measurements. CH_3CH_3 was a common reference compound in both experimental techniques to compare the corresponding results. The other reference compound was $CH_2=CH_2$, with well-known and comparable Cl atoms rate coefficient with HFIB. Note that both Cl atom reactions proceed via an association mechanism, and therefore their rate coefficients are temperature and pressure dependent. The rate coefficient for the reference reaction was taken by interpolation of the non-linear fit of the data, and has higher uncertainty. Similarly to OH rate coefficients, no substantial pressure dependence is expected in that relatively high pressure regime (approaching the high pressure limit). Thus, the kinetic results from the two independents facilities measured at 700 and 760 Torr can be treated and analyzed together and the quoted value is referred to 1 atm without any pressure correction. Adopting a linear least squares fit of the data, and forcing the fits to pass through zero (since intercepts were always negligible) obtained the Cl reaction rate coefficient, which was k_2(296 K, 1 atm) = (3.45 ±0.10) $\times 10^{-11}$ cm^3 $molecule^{-1}$ s^{-1}. The quoted error limits are at 95 % level of confidence and refers to the precision of the fit, which also includes the error limits of the independent measurements. Although the precision of relative rate measurements is very high (figure 3), it is worth to note that the rate coefficients obtained using the relative rate method depends strongly on the inherent systematic uncertainty of the selected reference reactions. Therefore, the ratio r_o is also given in table 1 and the errors in the k_1 and k_2 including the systematic uncertainties are presented in the subsection of kinetics in Discussion.

3.3 O_3 Kinetics

To the best of our knowledge, the present rate coefficient value for the reaction of O_3 with HFIB is the first in the literature. The O_3 kinetics was investigated under pseudo-first-order conditions for both HFIB and O_3. However, due to possible multiple pathways of the O_3 loss or concentration drop inside the chamber, e.g., dilution, we decided to maintain pseudo-first-order kinetic conditions for O_3 (in excess) and monitor HFIB decays. Any dilution or other first order dark losses of HFIB were measured in separate experiments, in the absence of O_3. The pseudo-first-order rate coefficient that represents HFIB concentration drop, due to other than reaction with O_3 processes was determined to be k_{other} =(6.36 ±0.15) $\times 10^{-6}$ s^{-1}, where the quoted uncertainty is the 2σ precision of the fit. The loss rate of HFIB is given:

$$\frac{d[HFIB]}{dt} = k_3[O_3][HFIB] + k_{other}[HFIB] \quad (11)$$

while for O_3 excess ($k_3 \times [O_3] = k_3'$) leads to:

$$ln\frac{[HFIB]_t}{[HFIB]_0} = (k_3' + k_{other})[HFIB] \quad (12)$$

Figure 4 depicts the pseudo-first-order decay plots of HFIB at high O_3 concentrations (i.e., (~37.2 – 44.6) $\times 10^{13}$ molecule cm^{-3}) that yields a total rate coefficient k_3' = (5.95 ±0.12) $\times 10^{-6}$ s^{-1}, which is identical to the dilution and other first-order losses of HFIB (k_{other}), within experimental precision. Since no HFIB reactivity was observed even at high O_3 concentrations, an upper limit for the rate coefficient of the O_3 reaction with HFIB was found to be $k_3 < 9.0 \times 10^{-22}$ cm^3 $molecule^{-1}$ s^{-1}, considering the marginal difference between dark and reaction loss rate of HFIB. Note that any conversion of O_3 to OH radicals would lead to a faster HFIB loss and to even lower upper limit for the reaction rate coefficient of O_3 with HFIB. However, since no HFIB reactivity was observed in our chamber experiments there was no need for OH scavengers. .

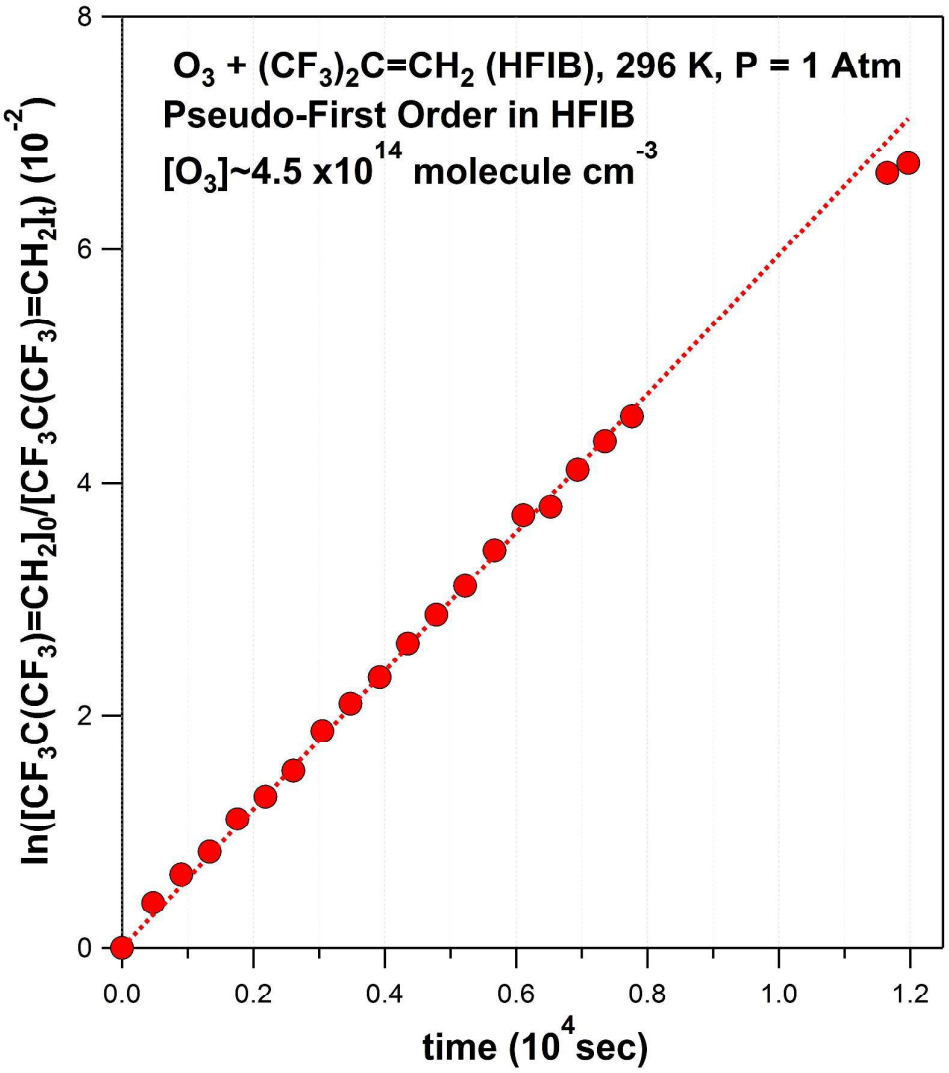

Figure 4. HFIB first order decay plot in the presence of O_3. The HFIB loss rate was independent of dilution or any other first-order dark losses of HFIB, leading to an upper limit for the O_3 rate coefficient k_3(296 K, 1 atm) < 9.0×10^{-22} cm^3 $molecule^{-1}$ s^{-1}.

3.4 IR Spectra and cross-sections

The infrared absorption spectra of HFIB were measured at 296 K using FTIR spectroscopy with a spectral resolution of 1 cm^{-1}. The IR spectra obeyed the Beer's law, ±1% precision, leading to linear dependence between absorbance and concentration with negligible intercept, i. e., <1 %. Total pressure inside the optical cell was varied between 10 and 100 Torr (He) without any pressure dependence. Figure 5 shows the HFIB absorption spectrum in the atmospherically more relevant wavenumber range, i. e., 600–1600 cm^{-1}. Strong absorption features were observed in

this region, in consistence with most fluorinated compounds. The peak cross section at 1197 cm^{-1} was (3.21 ± 0.10) $\times 10^{-18}$ cm^2 $molecule^{-1}$, and the integrated band strength (IBS) over the most relevant to the atmosphere range, 600–1600 cm^{-1}, was (2.27 ± 0.07) $\times$ 10^{-16} cm^2 $molecule^{-1}$ cm^{-1}. The quoted uncertainties include estimated systematic errors. The infrared spectra are provided in digital form in the Supplemental Material (Table S2).

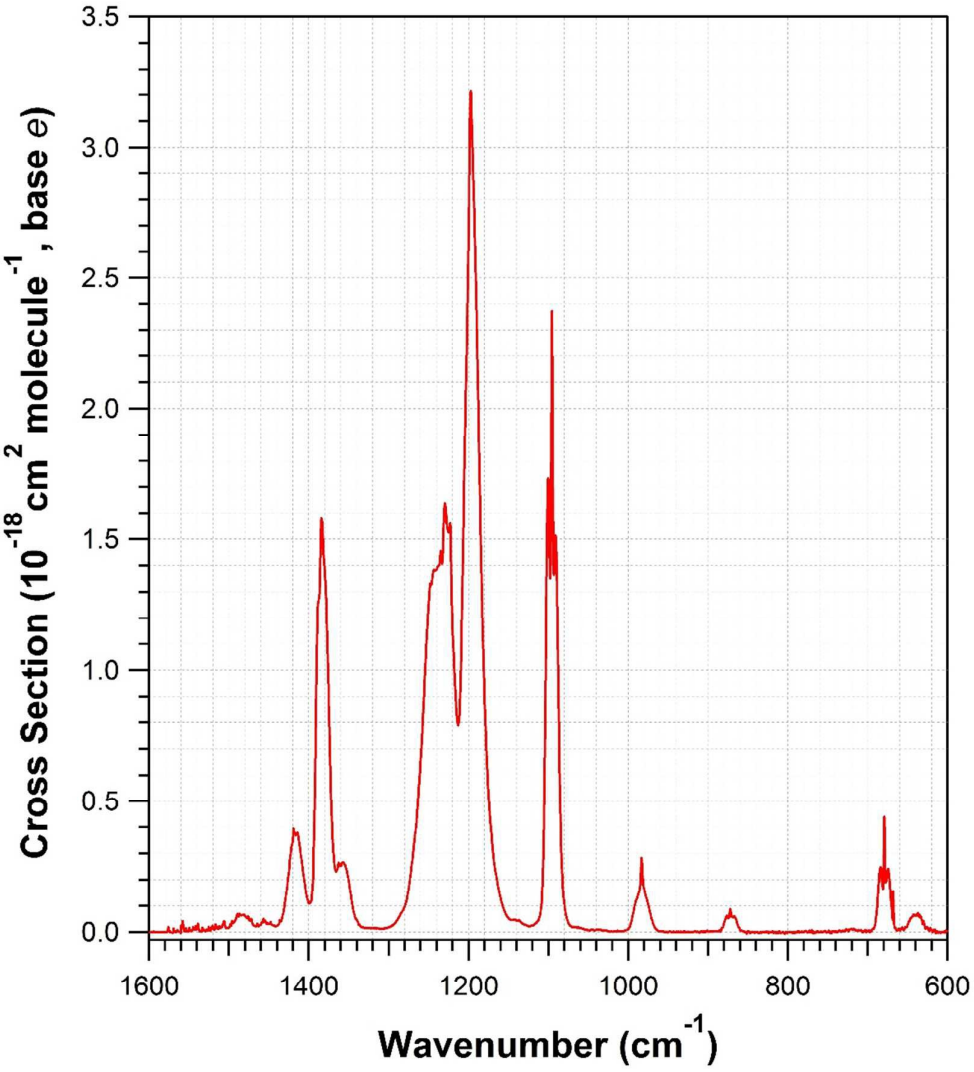

Figure 5. IR cross section spectrum of $(CF_3)_2C=CH_2$ recorded at 296 K and 1 cm^{-1} resolution.

3.5 OH radicals and Cl atoms initiated oxidation end-products

Figure 6 (a)-(c) shows the IR spectra of the reaction mixture in the Cl-initiated oxidation of HFIB and for the absence of reference compounds. In particular, the IR

spectrum prior to laser photolysis is shown in panel (a), after photolysis and substantial reactant conversion in panel (b), and last for complete reactant conversion in panel (c). Panel (d) shows the reference IR spectrum of hexafluoro-acetone. Panels (b) and (c) show the presence of the CO vibration band centered at 2146 cm^{-1}, and the P, Q and R branches around ~1783 cm^{-1} that correspond to HC(O)Cl.[16] CO could be formed either via thermal decomposition of HCHO or via reactions of Cl atoms with HCHO and/or HC(O)Cl. The observation of CO peak in the OH-initiated oxidation of HFIB verifies the formation of HCHO in both atmospheric oxidation schemes. Moreover, separate experiments were performed in the absence of laser light and by recording sequential spectra after substantial and complete reactant conversion. It was found that the HCl formation was increasing, which indicates an additional source of HCl formation, besides the Cl atom reactions with HCHO and HC(O)Cl primary end-products. Such HCl source could be the thermal decomposition of HC(O)Cl, which also leads to the formation of CO. However, the higher rate of CO increase compared to that of HCl, clearly demonstrates that there is an additional pathway of CO formation, suggesting that HCHO was also formed in Cl-initiated experiments either in presence or absence of NOx.

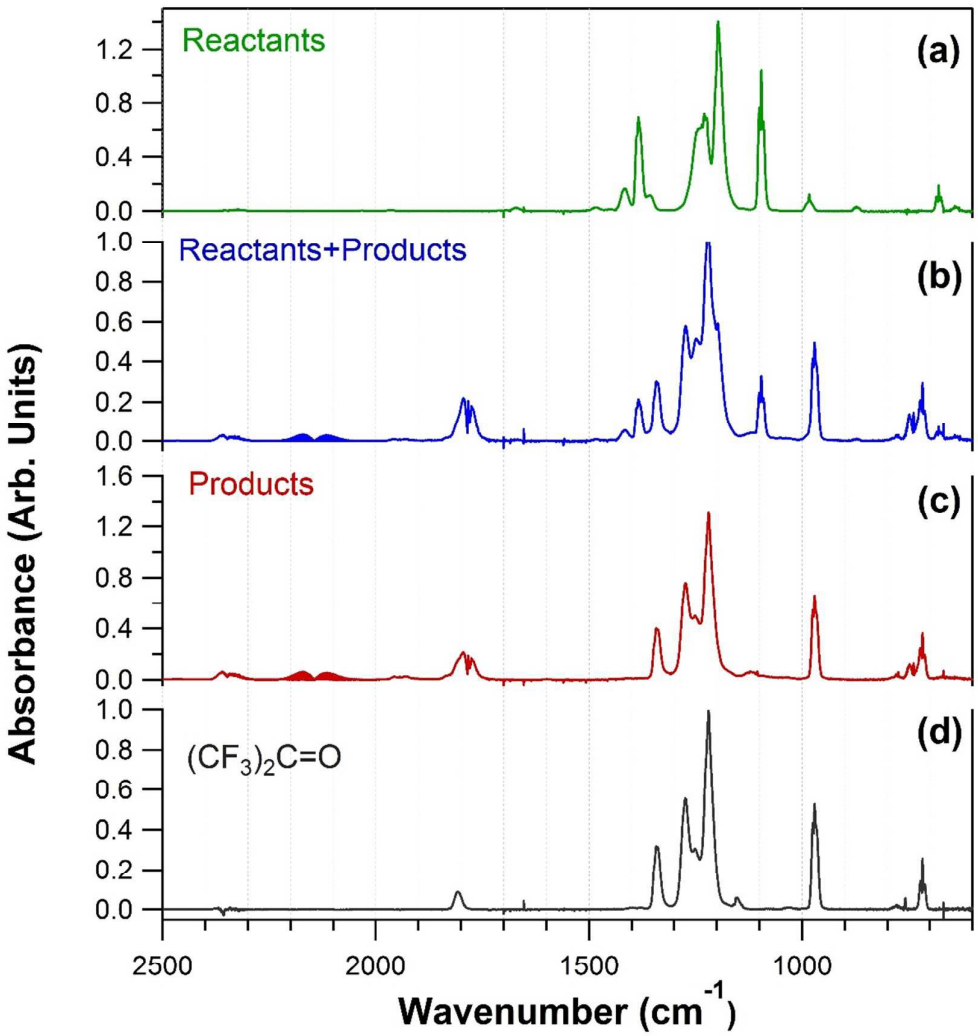

Figure 6. IR spectra of the reaction mixture in the Cl-initiated oxidation of HFIB and in the absence of reference compound: a) prior to laser photolysis, b) at partial conversion of reactants, c) at complete conversion of reactants, and d) $(CF_3)_2C(O)$ reference spectrum at 1 cm^{-1} resolution.

The observed end-products suggest that all reactions proceed mainly via an electrophilic addition to the unsaturated double bond, in agreement with previous kinetic studies with other HFOs.[16, 18, 19, 21, 22, 34, 36, 40] Figure 7 presents a simplified atmospheric oxidation scheme of HFIB initiated by Cl atoms and based on the above end-products analysis.

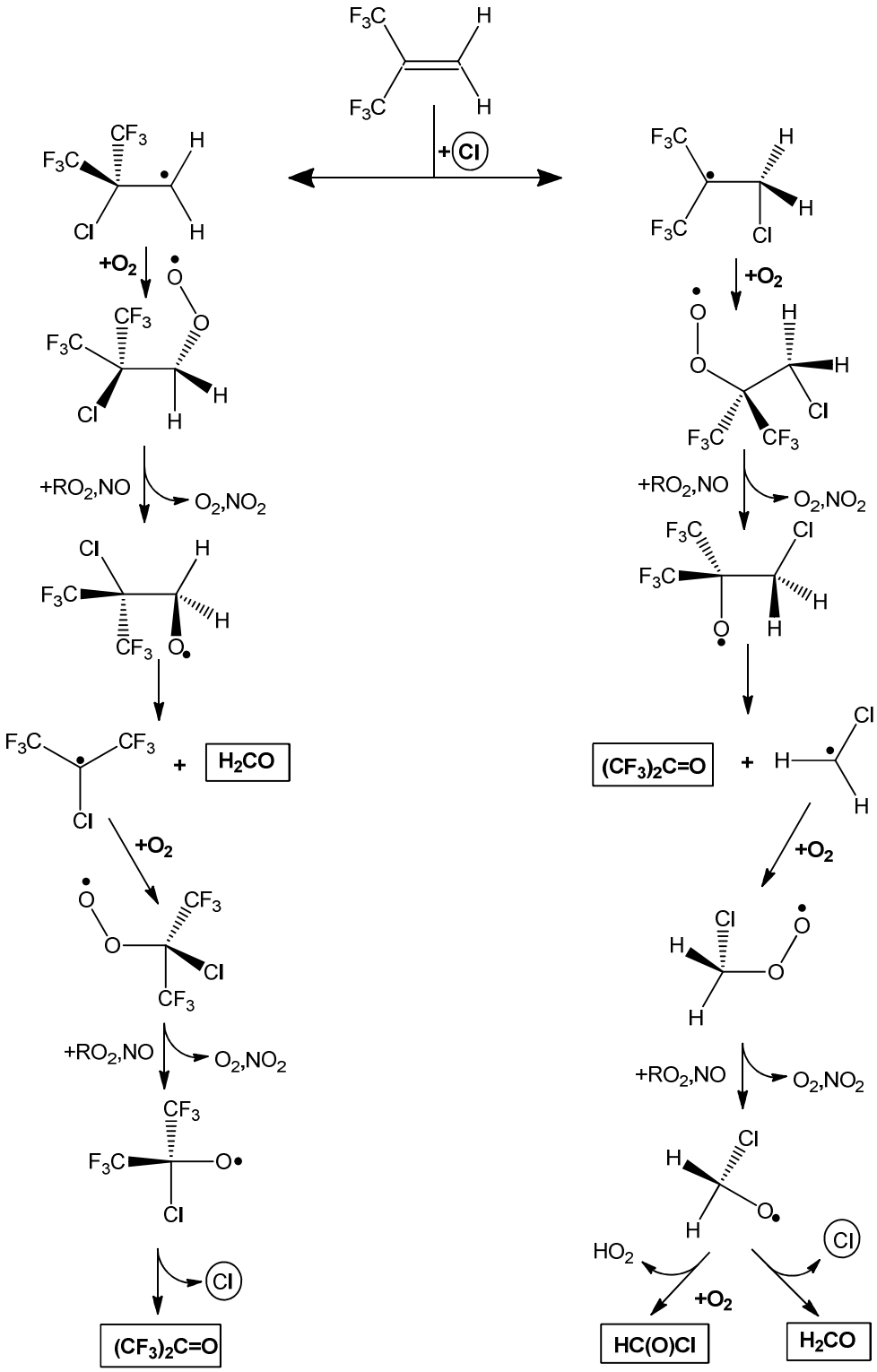

517

518 **Figure 7.** Simplified atmospheric oxidation scheme of $(CF_3)_2C=CH_2$. Major end-
519 products are noted in squares.

520

521 **3.6 Error Analysis**

The precision, repeatability and reproducibility, of OH and Cl atom relative rate coefficient measurements were tested by using two independent experimental setups and were proven high. Several experiments with each reference compound were carried out in both facilities, by selecting different spectral bands and peaks for monitoring HFIB and reference losses. HFIB impurity levels, <1.2 %, as determined using NMR spectroscopy, are not expected to affect relative rate determinations, since it is highly unlikely for compounds with similar degree of fluorination to have significantly higher IR cross sections than HFIB, and significantly and systematically interfere with HFIB in C-F absorption region, especially considering HFIB symmetry. It is worth to note, that although the impurity was not identified, a higher degree of fluorination would have resulted in higher purity levels in NMR analysis and thus the effect in bands interference would have been canceled out. However, to further test any impurity interference in the selected bands that HFIB was monitored, multiple bands were simultaneously monitored in absence of the reference compounds, in order to compare their relative loss. Different bands loss rate were identical, within 1 %, showing that HFIB impurities have a negligible effect, if any. Moreover, the selected spectral bands for kinetic analysis were free of reaction products features, as well, enabling highly precise measurements, better than ±2%. In addition, the rate coefficients obtained using three different reference compounds and two independent lab facilities were in agreement within ~3%. Probable systematic errors stemming from the corresponding errors in the rate coefficients of the reference reactions were minimized using several well-established reference reactions that were checked in both laboratories. Therefore, the precision of our rate coefficient measurements was on the order of 3%, while the overall absolute uncertainty is estimated to be ~7% or less, which includes the uncertainty in the reference reaction rate coefficients.

4. Discussion

4.1 Kinetics

During the course of this study Tovar *et al*. measured the relative rate coefficients for the title reactions at 298 K and 760 Torr of synthetic air by using a reaction chamber, and reported the values $k(OH+(CF_3)_2C=CH_2) = (6.58 \pm 2.25) \times 10^{-13}$ and $k(Cl+(CF_3)_2C=CH_2) = (3.50 \pm 0.85) \times 10^{-11}$ cm^3 molecule^{-1} s^{-1}.[34] Although the Cl rate coefficient value is identical to that of Tovar et *al*., within experimental precision, the OH rate coefficient value is ~17 % higher compared to the one of Tovar *et al*.. It

should be noted that the uncertainty of Tovar *et al*. value was ~34 %. Although our value lies within their error limits, theirs is not encompassed in our 2σ uncertainty, even including the estimated systematic errors, which results in k_1(296 K, 1 atm) = (7.82 ± 0.55) $\times 10^{-13}$ cm^3 $molecule^{-1}$ s^{-1} and k_2(296 K, 1 atm) = (3.45 ± 0.24) $\times$ 10^{-11} cm^3 $molecule^{-1}$ s^{-1}, respectively. The reason of such marginal difference between OH rate coefficients is unknown, although the relatively high uncertainty in their value is mainly due to the high error limits of reference reaction and the substantial scattering of their data.

4.2 Atmospheric Implications

4.2.1 Tropospheric lifetimes

The atmospheric loss of HFIB is expected to occur via the gas-phase reactions with the dominant oxidative species in the troposphere, i. e., OH radicals, Cl atoms, NO_3 radicals and O_3, and via the heterogeneous wet and dry deposition losses. Due to the low absorption cross-sections of hydrofluoroolefins (HFO), within the actinic spectrum region,[18] photolysis is not expected to contribute significantly in the removal of HFIB from the troposphere. NO_3 radicals might also be an important sink, particularly in night chemistry, since it is known that association reactions might be relatively fast processes and NO_3 radicals relative abundance is quite high.[41-44] However, Papadimitriou *et al*.[16], have shown that NO_3 chemistry does not have an important contribution to the atmospheric oxidation of CF_3CF_2=CH_2 and a similar behavior is expected for HFIB. The latter argument may also be supported by the similar molecular structure of both compounds, since one –F atom in CF_3CF_2=CH_2 has been replaced by a –CF_3 group in HFIB. Taking into account that –F atom and –CF_3 group are characterized by similar electron withdrawing effects, [34, 45] the electronic density of the double bond is expected to have similar distribution and the reactivity towards NO_3 radicals to be similar too. On the top of that, the increased size of –CF_3 group compared to the –F atom is expected to lead to an increased steric hindrance compared to –F atoms and to a further decrease in reactivity of HFIB towards NO_3 radicals. Therefore, we conclude that NO_3 radicals are not expected to have a significant effect in tropospheric lifetime of HFIB. Another potential gas phase loss of HFIB could be the reaction with O_3. As noted in O_3 kinetics section, due to the lack of kinetic data for the O_3 reaction with HFIB, in the literature, the present results

cannot be compared with other studies. For an average O_3 concentration of 35 ppb[46] and an upper limit value of $k_3 < 9.0 \times 10^{-22}$ cm^3 molecule^{-1} s^{-1}, a lower limit of lifetime ~41 years was estimated using the expression $\tau_{O_3} = \frac{1}{k_{O_3}[O_3]}$. The latter suggests that the O_3 chemistry constitutes a negligible atmospheric sink of HFIB. On the other hand both OH radicals and Cl atoms lead to a rapid decomposition of HFIB and thus those two processes were considered as the dominant reactions for the gas phase degradation of HFIB in the troposphere, which also determine the tropospheric lifetime of HFIB. However, it is worth to note that HFIB is a relatively short-lived compound and thus it is expected that its lifetime is mainly governed by regional emissions and it is very difficult to be determined globally. In this work we have estimated HFIB local lifetime using the expression $\frac{1}{\tau_{local}} = \frac{1}{\tau_{OH}} + \frac{1}{\tau_{Cl}}$, where $\tau_{OH} = \frac{1}{k_{OH}[OH]}$ and $\tau_{Cl} = \frac{1}{k_{Cl}[Cl]}$, using as [OH] and [Cl] the average concentration in the free troposphere, $[OH]_{avg} = 10^6$,[47, 48] and $[Cl]_{avg} = 10^4$ molecule cm^{-3}.[49, 50] It is worth noting that there is currently a large uncertainty in Cl atmospheric concentration levels and the above average Cl concentration can be considered as a local maximum, representative though, for the regions, where HFIB emissions are expected to be higher. Therefore, the local OH lifetime was estimated to be ~15 days, while the local Cl lifetime is ~34 days. The effective local lifetime including both OH and Cl chemistry was estimated to be ~10.3 days. The latter demonstrates the importance of the Cl chemistry to the atmospheric oxidation of HFIB (~30% lower lifetime) and to unsaturated fluorocarbons in general, in agreement with Papadimitriou *et al*..[16, 18] The substantially more rapid degradation of HFOs induced by Cl atoms, which is in the order of some decades to hundred times faster than OH radicals, may compensate for the Cl non-well mixing and the lower mixing ratios in the atmosphere. Moreover, for such short-lived compounds with the highest emissions expected in large cities, the Cl contribution might be even more important, since the highest Cl levels have been detected in polluted areas and in the marine boundary layer (MBL), where most metropolitans are located. It is worth to note that the reported Cl average concentrations in MBL are 1.3×10^5 molecule cm^{-3},[50] and thus Cl importance is expected to be even higher in those regions.

620 **4.2.2 Radiative Efficiency (RE), Global Warming Potentials (GWPs) and**
621 **Estimated Photochemical Ozone Creation Potential (ε^{POCP})**
622 Radiative efficiency (RE) of HFIB was estimated using the IR spectra and the lifetime
623 estimations at 296 K obtained in this study by employing the approximation method
624 developed from Pinnock *et al*..[51] This approach is more appropriate for compounds
625 with diffuse absorption bands (like HFIB) and calculates REs for long-lived
626 compounds (LLC) with an estimated 10 – 15 %[52] uncertainty. Recently, Hodnebrog *et*
627 *al*.[53] revised the Pinnock *et al*.[51] model in order to improve the clouds representation
628 and the spatial atmospheric distribution of temperature and water vapor to scale
629 resolution 1 cm^{-1}. They also considered lifetime-dependent correction factors for
630 short-lived compounds (SLC), in order to include VOC that are not well mixed in the
631 troposphere. They estimated uncertainties of ca. 23 % for gases with lifetimes shorter
632 than 5 years and known IR absorption cross-sections. No significant difference in the
633 RE values was observed by adopting either model (<6%), and treating HFIB as LLC.
634 Thus we report only the results obtained using the Hodnebrog *et al*. [53] model and we
635 calculated RE by taking into account only the OH chemistry (RE(OH)), as well as
636 including the Cl chemistry (RE(eff)). Therefore, HFIB radiative efficiency was found
637 to be RE(LLC) =0.254 W m^{-2} ppb^{-1} (Pinnock *et al*.[51]: 0.270 W m^{-2} ppb^{-1}) considering
638 HFIB as LLC. Taking into account lifetime correction factors we calculated the
639 radiative efficiencies to be RE(SLC,OH) =0.033 W m^{-2} ppb^{-1}, considering a lifetime-
640 dependent factor of 0.13 and solely the OH chemistry. In addition, RE(SLC,eff)
641 =0.024 W m^{-2} ppb^{-1} by including the Cl chemistry, which corresponds to a ca. 28 %
642 decrease. The global warming potentials (GWP) of HFIB for the 20, 100, and 500
643 year-time horizons are given in Table 3, along with the REs and the estimated
644 lifetimes.
645
646 **Table 3.** Lifetimes, Radiative efficiencies and Global Warming Potentials of HFIB

Lifetime (days)		**Radiative Efficiency (W m^{-2} ppb^{-1})**					
τ_{OH}	14.8	**LLC[a]**		**SLC(OH)[b]**		**SLC(eff)[c]**	
		0.254		0.033		0.017	
τ_{Cl}	33.5	**GWP, OH (eff)[d]**					
		Time Horizon (years, LLC)			**Time Horizon (years, SLC)**		
		20	**100**	**500**	**20**	**100**	**500**

τ_{eff}	10.3	14.3 (9.9)	4.1 (2.8)	1.2 (0.8)	1.9 (1.0)	0.6 (0.3)	0.2 (0.1)

[a] LLC stands for long lived compound
[b] SLC stands for short lived compounds and OH denotes the parameters estimates taking into account only OH tropospheric removal of HFIB
[c] eff denotes the parameters estimates including both OH and Cl processing of HFIB in the troposphere
[d] GWPs in parentheses refer to the values including the Cl chemistry

Our GWP calculations used the same integrated radiative forcing of CO_2 as in WMO 2007, and the obtained values are given in Table 3, which may be compared with the GWP values reported by WMO 2007. The GWPs for HFIB treated as LLC are GWP(OH)=4.1 and and GWP(eff)=2.8, excluding and including Cl chemistry, respectively, for a hundred year-time-horizon. Treating HFIB as SLC resulted in even lower GWPs by a factor of 7 to 8, for the same time horizon. Although HFIB emissions to the atmosphere are currently unknown, the short atmospheric lifetime and low GWP of HFIB will lead to minor impact to global warming and climate change, unless HFIB emissions become significantly high. Finally, the ε^{POCP} was calculated by adopting the Jenkin[54] and Derwent *et al.*[55] method that is based only on the molecular properties of considered compounds and their reactivity towards OH radicals. ε^{POCP} estimates the total incremental ozone increase in a multi-days modeling, as by-product of the atmospheric oxidation of hydrocarbons, relative to ethene, in the same mass basis. The expression used was:

$$\varepsilon^{POCP} = a_1 \times \gamma_S \times \gamma_R^{\beta}(1 - a_2 \times n_C) \qquad (13)$$

where a_1, β and a_2 are the fit parameters obtained by plotting POCP versus ε^{POCP} for similar VOC, γ_S is the structure based ozone index ($\gamma_S = (n_B/M)\times(28/6)$), γ_R^{β} is the relative OH reactivity of the VOC compared to ethane ($(\gamma_R^{\beta} = (k_{OH}/n_B)\times(6/8.64\times10^{-12})$), M is the molecular mass, n_B is the number of C-C and C-H bonds and n_C is number of carbons. For reactions with k_{OH} between $(0.4 - 4) \times10^{-12}$ cm^3 molecule^{-1} s^{-1}, the suggested β value is 0.5, while a_1 and a_2, are not defined for that reaction rate coefficients range of alkenes, and thus a_1 was calculated normalizing alkanes behavior to alkenes for intervals β = 0.25 and 0.5, leading to an increase of ~17 % and to an a_1 =124.8. a_2 is not very sensitive and since no change was determined in alkanes for 0.25 and 0.5 intervals, a similar trend was assumed for alkenes; thus, the value of a_2 = 0.03 was used in the above expression. Using the OH rate coefficient, the estimated

680 photochemical ozone creation potential of HFIB was calculated to be ε^{POCP}(HFIB) =
681 4.60, which is in the same order of similar HFO and significantly lower than non-
682 fluorinated unsaturated hydrocarbons.[56] However, it is worth to note that for certain
683 compounds and at local scale, the Cl-initiated oxidation may be of equal importance
684 to the OH-initiated oxidation, especially over regions with high emissions, such as
685 coastal regions and polluted areas with rather high Cl atoms mixing ratios. In such
686 cases, the Cl chemistry should be also considered, and this may lead to higher POCP
687 values.
688
689 **4.2.3 Impact of Atmospheric Oxidation End-Products**
690 The atmospheric lifecycle assessment of HFIB requires knowledge of the end-
691 products analysis, the mechanism of atmospheric degradation and the overall impact
692 to the atmosphere. The IR end-product analysis revealed that the dominant oxidation
693 end-products were hexafluoroacetone ($(CF_3)_2C(O)$) and formaldehyde (HCHO) for
694 both OH and Cl initiated atmospheric oxidation. In addition, formyl chloride
695 (HC(O)Cl) was also identified as end co-product in the Cl-induced tropospheric
696 oxidation. $(CF_3)_2C(O)$ is not expected to be removed from the atmosphere via gas-
697 phase reactions, but most likely via heterogeneous wet and/or dry deposition
698 processes. Therefore, $(CF_3)_2C(O)$, will most likely lead to trifluoroacetic acid (TFA)
699 formation, which although cannot alter the global atmospheric budget, it is necessary
700 to identify and quantify its sources, in order to provide a better evaluation of non-
701 biogenic sources.[18, 57] HCHO atmospheric lifetime is estimated to a few hours and the
702 major sinks are photolysis and OH- and Br-initiated gas phase chemistry,[58] producing
703 CHO radical, which subsequently will be converted to CO and HO_2. However, HCHO
704 atmospheric abundance is primarily governed by the CH_4 budget and the oxidation
705 processes, therefore HFIB can only have a negligible contribution to HCHO
706 atmospheric budget. Finally, HC(O)Cl, was identified as oxidation end-product in the
707 Cl-initiated reaction, similarly to what Papadimitriou *et al.*[16] has observed for the
708 reaction of Cl atoms with $CF_3CF=CH_2$. As it has been discussed, HC(O)Cl has a short
709 lifetime of ~1 month and cannot affect the Cl load of the stratosphere, significantly.
710 However, other, more stable, chlorinated end-products of Cl initiated oxidation
711 reactions of unsaturated hydrocarbons can potentially act as tropospheric Cl carriers
712 into the stratosphere. Thus, the atmospheric oxidation of non-ozone depletion
713 substances (non-ODSs) may lead to stable ODSs that may lead to indirect threat to the

stratospheric ozone layer. Therefore, hydrofluoroolefins (HFO), the most recent CFC alternatives, need a case-by-case thorough kinetic study before their mass-scale production and use.

5. Conclusions

In the present work, the OH radicals, Cl atoms and O_3 gas phase kinetics towards hexafluoroisobutylene (HFIB, $(CF_3)_2C=CH_2$) were studied at 296 K and 1 atm of synthetic air. The Cl rate coefficient, k_2(296 K, 1 atm) = (3.45 ±0.10) $\times 10^{-11}$ cm^3 $molecule^{-1}$ s^{-1}, was determined to be ~44 times higher compared to the OH rate, k_1(296 K, 700 Torr) = (7.82 ±0.30) $\times 10^{-13}$ cm^3 $molecule^{-1}$ s^{-1}. The upper limit of the O_3 rate coefficient was, k_3(296 K, 760 Torr) < (9.0 ± 0.3) × 10^{-22} cm^3 $molecule^{-1}$ s^{-1}, which demonstrates that the O_3 chemistry has a negligible impact in atmospheric lifetime of HFIB. Although the OH chemistry is expected to be predominant in the tropospheric gas phase degradation of HFIB, the Cl chemistry should also be included in the model calculations, especially in regions with elevated levels of Cl atoms, such as coastal and polluted urban areas, where HFIB emissions may be high. The average HFIB lifetime was determined to be ~14.8 days, considering only the OH chemistry and ~10.3 days by including the Cl chemistry. The 30 % reduction of atmospheric lifetime by including the Cl chemistry, affects several critical atmospheric parameters, such as radiative efficiency (RE), global warming potential (GWP) and mainly photochemical ozone creation potential (POCP). The RE and GWP of HFIB were estimated using the obtained IR cross-sections and average lifetimes, and treating HFIB as LLC or SLC. In all cases, it was found a decrease of 50 % for both RE and GWP by including the Cl chemistry. It is worth to note that although HFIB is a highly fluorinated olefin, it has short atmospheric lifetime that leads to low GWP and therefore is expected to have a minor impact to global warming and climate change. In addition, ε^{POCP} was calculated based on the molecular properties of HFIB and OH reactivity, and was found to be ~5, which is in the same range with POCPs of similar structure HFOs and substantially lower than that of non-fluorinated unsaturated hydrocarbons, e. g., ethene and isopropylene. However, it is important to consider the influence of Cl reactivity to POCP, especially considering that the atmospheric impact of short lived compounds, such as HFIB, will be more local than global and their main emissions would be in areas with increased levels of Cl atoms. On top of that, Cl

747 reactions with HFOs are typically 10-100 times faster than OH reactions, in
748 comparison with alkanes that Cl initiated oxidation might be of minor importance,
749 since OH reactions are ~10 times slower or less and they are ~ 100 time more
750 abundant. Finally, the oxidation end-products of HFIB were $(CF_3)_2C(O)$ and HCHO,
751 as well as HC(O)Cl in the Cl initiated scheme. Both $(CF_3)_2C(O)$ and HCHO are
752 expected to have a minor impact to atmospheric chemistry, considering that their
753 degradation products have not a substantial input to the atmospheric budgets of TFA,
754 HCHO or CO. On the other hand, HC(O)Cl formation indicates that Cl association
755 reactions with HFOs (non-ODSs) may lead to ODSs formation. However, the impact
756 of HC(O)Cl to ozone depletion is expected to be minor, considering its short lifetime,
757 as well as the short lifetime of HFIB (degradation in lower troposphere), which limits
758 the transfer of tropospheric Cl budget to the stratosphere. Hence, in the selection of an
759 HFO as CFC substitute, it is also important to specify the amount of potentially stable
760 chlorinated by-products generated via Cl atoms oxidation, which may have negative
761 impact to the ozone layer.
762
763 **Acknowledgments**. This work was in part supported by the European Commission
764 within the EUROCHAMP2 project, the Labex Voltaire (ANR-10-LABX-100-01), and
765 by the Hellenic General Secreatariate for Research and Technolgy with the FORECO
766 project. We greatly acknowledge Assist. Prof. Apostolos Spyros for the $(CF_3)_2C=CH_2$
767 sample gas phase NMR characterization and analysis.
768
769

References

1. M. Molina and F. S. Rowland, *Nature*, 1974, 249, 810-812.
2. T. J. Wallington, W. F. Schneider, D. R. Worsnop, O. J. Nielsen, J. Sehested, W. J. Debruyn and J. A. Shorter, *Environ. Sci. Technol.*, 1994, 28, 320A-326A.
3. V. C. Papadimitriou, K. G. Kambanis, Y. G. Lazarou and P. Papagiannakopoulos, *J. Phys. Chem. A*, 2004, 108, 2666–2674.
4. V. C. Papadimitriou, A. V. Prosmitis, Y. G. Lazarou and P. Papagiannakopoulos, *J. Phys. Chem. A*, 2003, 107, 3733-3740.
5. J. G. Calvert, R. Atkinson, J. A. Kerr, S. Madronich, G. K. Moortgat, T. J. Wallington and G. Yarwood, *Mechanisms of the Atmospheric Oxidation of the Alkenes*, Oxford University, New York, 2000.
6. L. Vereecken, H. Harder and A. Novelli, *Phys. Chem. Chem. Phys.*, 2014, 16, 4039-4049.
7. J. Kalinowski, P. Heinonen, I. Kilpeläinen, M. Räsänen and R. B. Gerber, *J. Phys. Chem. A*, 2015, 119, 2318–2325.
8. T. Berndt, T. Jokinen, R. L. Mauldin, T. Petaja, H. Herrmann, H. Junninen, P. Paasonen, D. R. Worsnop and M. Sipila, *J. Phys. Chem. Lett.*, 2012, 3, 2892-2896.
9. M. D. Brynteson, C. C. Womack, R. S. Booth, S. H. Lee, J. J. Lin and L. J. Butler, *J. Phys. Chem. A*, 2014, 118, 3211-3229.
10. T. J. Preston, G. T. Dunning, A. J. Orr-Ewing and S. A. Vazquez, *J. Phys. Chem. A*, 2014, 118, 5595-5607.
11. D. L. Thomsen and S. Jørgensen, *Chem. Phys. Lett.*, 2009, 481, 29-33.
12. E. W. Kaiser and T. J. Wallington, *J. Phys. Chem.*, 1996, 100, 9788-9793.
13. R. Atkinson, E. C. Tuazon and S. M. Aschmann, *Environ. Sci. Technol.*, 1995, 29, 1674-1680.
14. M. P. Andersen, O. J. Nielsen, M. D. Hurley and T. J. Wallington, *Phys. Chem. Chem. Phys.*, 2012, 14, 1735-1748.
15. V. L. Orkin, G. A. Poskrebyshev and M. J. Kurylo, *J. Phys. Chem. A*, 2011, 115, 6568-6574.
16. V. C. Papadimitriou, Y. G. Lazarou, R. K. Talukdar and J. B. Burkholder, *J. Phys. Chem. A* 2010, 115, 167-181.
17. M. Baasandorj, G. Knight, V. C. Papadimitriou, R. K. Talukdar, A. R. Ravishankara and J. B. Burkholder, *J. Phys. Chem. A*, 2010, 114, 4619-4633.
18. V. C. Papadimitriou, R. K. Talukdar, R. W. Portmann, A. R. Ravishankara and J. B. Burkholder, *Phys. Chem. Chem. Phys.*, 2008, 10, 808–820.
19. M. D. Hurley, T. J. Wallington, M. S. Javadi and O. J. Nielsen, *Chem. Phys. Lett.*, 2008, 450, 263–267.
20. R. Søndergaard, O. J. Nielsen, M. D. Hurley, T. J. Wallington and R. Singh, *Chem. Phys. Lett.*, 2007, 443, 199-204.
21. T. Nakayama, K. Takahashi, Y. Matsumi, A. Toft, M. P. S. Andersen, O. J. Nielsen, R. L. Waterland, R. C. Buck, M. D. Hurley and T. J. Wallington, *J. Phys. Chem. A*, 2007, 111, 909-915.
22. M. D. Hurley, J. C. Ball and T. J. Wallington, *J. Phys. Chem. A*, 2007, 111, 9789–9795.
23. M. P. S. Andersen, O. J. Nielsen, A. Toft, T. Nakayama, Y. Matsumi, R. L. Waterland, R. C. Buck, M. D. Hurley and T. J. Wallington, *.J. Photoch. Photobio. A*, 2005, 176, 124-128.

24. M. N. Mashino, Y.; Kawasaki, M.; Wallington, T. J.; Hurley, M. D., *J. Phys. Chem. A*, 2000, 104, 7255-7260.
25. G. Acerboni, J. A. Beukes, N. R. Jensen, J. Hjorth, G. Myhre, C. J. Nielsen and J. K. Sundet, *Atmos. Environ.*, 2001, 35, 4113-4123.
26. L.-l. Ai, X.-m. Duan and J.-y. Liu, *Comput. Theor. Chem.*, 2013, 1013, 15-22.
27. Y. Zhang, J. Sun, K. Chao, H. Sun, F. Wang, S. Tang, X. Pan, J. Zhang and R. Wang, *J. Phys. Chem. A*, 2012, 116, 3172-3181.
28. B. Dua, C. Feng and W. Zhang, *Chem. Phys. Lett.*, 2009, 479, 37-42.
29. K. Takahashi, E. Iwasaki, T. Nakayama, Y. Matsumi and T. J. Wallington, *Int. J. Chem. Kinet.*, 2007, 39, 328-332.
30. M. S. Javadi, R. Søndergaard, O. J. Nielsen, M. D. Hurley and T. J. Wallington, *Atmos. Chem. Phys.*, 2008, 8, 3141–3147.
31. L. Chen, T. Uchimaru, S. Kutsuna, K. Tokuhashi and A. Sekiya, *Int. J. Chem. kin.*, 2010, 42, 619-628.
32. M. S. Alam, A. R. Rickard, M. Camredon, K. P. Wyche, T. Carr, K. E. Hornsby, P. S. Monks and W. J. Bloss, *J. Phys. Chem. A*, 2013, 117, 12468-12483.
33. A. Sadezky, R. Winterhalter, B. Kanawati, A. Rompp, B. Spengler, A. Mellouki, G. Le Bras, P. Chaimbault and G. K. Moortgat, *Atmos. Chem. Phys.*, 2008, 8, 2667-2699.
34. C. M. Tovar, M. B. Blanco, I. Barnes, P. Wiesen and M. A. Teruel, *Atmos. Environ.*, 2014, 88, 107-114.
35. M. N. Romanias, V. G. Stefanopoulos, D. K. Papanastasiou, V. C. Papadimitriou and P. Papagiannakopoulos, *Int. J. Chem. Kin.*, 2010, 42, 724-734.
36. T. Kelly, V. Bossoutrot, I. Magneron, K. Wirtz, J. Treacy, A. Mellouki, H. Sidebottom and G. L. Bras, *J. Phys. Chem. A*, 2005, 109, 347-355.
37. S. P. Sander, J. Abbatt, J. R. Barker, J. B. Burkholder, R. R. Friedl, D. M. Golden, R. E. Huie, C. E. Kolb, M. J. Kurylo, G. K. Moortgat, V. L. Orkin and P. H. Wine, *Chemical Kinetics and Photochemical Data for Use in Atmospheric Studies, Evaluation No. 17" JPL Publication 10-6, Jet Propulsion Laboratory, Pasadena*, 2011
38. W. D. Taylor, T. D. Allston, M. J. Moscato, G. B. Fazekas, R. Kozlowski and G. A. Takacs, *Int. J. Chem. kin.*, 1980, 12, 231–240.
39. J. B. Burkholder and E. J. Bair, *J. Phys. Chem.*, 1983, 87, 1859–1863.
40. V. L. Orkin, L. E. Martynova and A. N. Ilichev, *J. Phys. Chem. A*, 2010, 114, 5967–5979.
41. B. J. Finlayson-Pitts and J. N. Pitts, Jr., *Chemistry of the Upper and Lower Atmosphere*, Academic Press, San Diego, 2000.
42. J. H. Seinfeld and S. N. Pandis, *Atmospheric Chemistry and Physics*, John Wiley & Sons, New York, 1998.
43. M. Vrekoussis, M. Kanakidou, N. Mihalopoulos, P. J. Crutzen, J. Lelieveld, D. Perner, H. Berresheim and E. Baboukas, *Atmos. Chem. Phys.*, 2004, 4, 169-182.
44. S. S. Brown and J. Stutzb, *Chem. Soc. Rev.*, 2012, 41, 6405-6447.
45. W. B. DeMore, *J. Phys. Chem.*, 1996, 100, 5813–5820.
46. S. Solomon, J. B. Burkholder, A. R. Ravishankara and R. R. Garcia, *J. Geophys. Res., [Atmos.]*, 1994, 99, 20929–20936.
47. S. A. Montzka, C. M. Spivakovshy, J. H. Butler, J. W. Elkins, L. T. Lock and D. J. Mondeel, *Science*, 2000, 288, 500–503.

48. R. G. Prinn, J. Huang, R. F. Weiss, D. M. Cunnold, P. J. Fraser, P. G. Simmonds, A. McCulloch, C. Harth, P. Salameh, S. O'Doherty, R. H. J. Wang, L. Porter and B. R. Miller, *Science*, 2001, 292, 1882–1888.
49. U. Platt, W. Allen and D. Lowe, *Atmos. Chem. Phys.*, 2004, 4, 2283–2300.
50. C. W. Spicer, E. G. Chapman, B. J. Finlayson-Pitts, R. A. Plastridge, J. M. Hubbe, J. D. Fast and C. M. Berkowitz, *Nature*, 1998, 394, 353–356.
51. S. Pinnock, M. D. Hurley, K. P. Shine, T. J. Wallington and T. J. Smyth, *J. Geophys. Res.*, 1995, 100, 23227–23238.
52. V. C. Papadimitriou, M. R. McGillen, S. C. Smith, A. M. Jubb, R. W. Portmann, B. D. Hall, E. L. Fleming, C. H. Jackman and J. B. Burkholder, *J. Phys. Chem. A* 2013, 117, 11049−11065.
53. Ø. Hodnebrog, M. Etminan, J. S. Fuglestvedt, G. Marston, G. Myhre, C. J. Nielsen, K. P. Shine and T. J. Wallington, *Rev. Geophys.* , 2013, 51, 300-378.
54. M. E. Jenkin, *Photochemical Ozone and PAN Creation Potentials: Rationalisation and Methods of Estimation. AEA Technology plc, Report AEAT-4182/ 20150/003, AEA Technology plc. National Environmental Technology*, Centre, Culham, Oxfordshire OX14 3DB, UK, **1998**.
55. R. G. Derwent, M. E. Jenkin, S. M. Saunders and M. J. Pilling, *Atmos. Environ.*, 1998, 32, 2429-2441.
56. T. J. Wallington, M. P. S. Andersen and O. J. Nielsen, *Atmos. Environ.*, 2010, 44, 1478-1481.
57. J. C. Boutonnet, P. Bingham, D. Calamari, C. D. Rooij, J.Franklin, T. Kawano, J.-M. Libre, A. McCulloch, G. Malinverno, J. M. Odom, G. M. Rusch, K. Smythe, I. Sobolev, R. Thompson and J. M. Tiedje, *Hum. Ecol. Risk Assess.*, 1999, 5, 59-124.
58. R. A. Salmon, S. J.-B. Bauguitte, W. Bloss, M. A. Hutterli, A. E. Jones, K. Read and E. W. Wolff, *Atmos. Chem. Phys.*, 2008, 8, 4085–4093.